



Enhanced dielectric and mechanical properties of epoxy-cyanate ester resin by Al₂O₃ and OMMT

Zhiguo Li¹ · Yufei Chen^{1,2} · Yulong Liu¹ · Chengjun Teng³ · Simin Chen¹ · Weiwei Cui¹

Received: 14 January 2020 / Accepted: 10 April 2020 / Published online: 18 April 2020
© Springer Science+Business Media, LLC, part of Springer Nature 2020

Abstract

In order to achieve the purpose of simultaneously improving the mechanical properties and dielectric properties of biscyanatophenylpropane (BCE), a copolymer of bisphenol A epoxy resin (E51) and (BCE) was used as the matrix resin (E51-BCE), and Al₂O₃ with sol–gel method and the organically montmorillonite (OMMT) were used as the reinforcements to prepare the Al₂O₃/OMMT/E51-BCE composites. The structure of Al₂O₃ was identified to be γ -Al₂O₃ by X-ray diffraction (XRD) and transmission electron microscope (TEM), and MMT was organically modified by intercalation agent octadecyl trimethyl ammonium chloride (OTAC) to obtain OMMT and characterized by Fourier-transform infrared spectrometer (FT-IR), thermogravimetric analysis (TGA) and scanning electron microscope (SEM). The results showed that the interlayer spacing of OMMT (2.14 nm) was bigger than that of MMT (1.44 nm), with an increase of about 48.6%. The results indicated that both Al₂O₃ and OMMT can improve the dielectric properties and mechanical properties of the composite materials. The Al₂O₃/OMMT/E51-BCE composites are found to have the best performance; the bending strength, bending modulus and impact strength were 187.34 MPa, 3.59 GPa and 35.12 kJ m⁻², respectively, when the content of Al₂O₃ and OMMT are all 2 wt%. And the dielectric constant, dielectric loss tangent, breakdown strength and volume resistivity of the composites reached peak values of 3.4, 0.005, 19.53 kV mm⁻¹ and $8.9 \times 10^{14} \Omega$ m, respectively. The overall performance of the composite fulfilled the basic requirements of electrical and insulating materials and could expand application of BCE material in many areas.

1 Introduction

In recent years, cyanate ester resin (CE) has become an excellent material for radomes, high-quality circuit board substrates and structural materials for its low dielectric constant, low dielectric loss, high heat resistance and high strength [1, 2]. And, it is usually modified with inorganic nanomaterials or other resin materials, in order to further improve the dielectric and mechanical properties of CE [3–5].

The epoxy resin (EP) is an ideal copolymerization modification material to CE, as its long aliphatic chain segments can enhance the toughness of CE in a way of reducing the regularity of the CE molecular structures [6]. And, the nano-Al₂O₃ is a kind of modifying material, due to its stable covalent bond structure and good dielectric property [7, 8], while its high surface activity and absorptivity can form a strong interfacial interaction with the matrix resin [9–11]. According to previous studies, two-dimensional (2D) layered montmorillonite (MMT) has better toughening and reinforcing effect on resin materials compared with the zero-dimensional (0D) nanoparticles [12–14]. However,

✉ Yufei Chen
chenyufei@hrbust.edu.cn

Zhiguo Li
lizhiguo9503@gmail.com

Yulong Liu
375976129@qq.com

Chengjun Teng
810025406@qq.com

Simin Chen
1518130025@qq.com

Weiwei Cui
cuiww@hrbust.edu.cn

¹ School of Materials Science and Engineering, Harbin University of Science and Technology, Harbin 150040, China

² Key Laboratory of Engineering Dielectrics and Its Application, Ministry of Education, Harbin University of Science and Technology, Harbin 150080, China

³ Harbin Xiangfang District Center for Disease Control and Prevention, Harbin 150030, China

the unmodified MMT layers contain many metal cations, which make the MMT exhibit strong hydrophilicity and poor compatibility with matrix resin. Although organic modification of MMT can improve the compatibility with the matrix resin by replacing the metal cations between the MMT layers with organic molecules to obtain composite materials with excellent mechanical properties, still, the organic MMT is not conducive to reducing the dielectric constant of the composite [15–17]. A new solution is needed.

In this paper, a copolymer of CE and EP was used as the matrix resin, and been modified by Al_2O_3 prepared by the sol-gel method and the organically MMT (OMMT). The structure of Al_2O_3 , OMMT and the composites was characterized by FT-IR, XRD, SEM and TEM, and the mechanical and dielectric properties of the composites were studied. These results provided certain value to further expand the application of BCE resin matrix composite.

2 Experimental

2.1 Materials

Biscyanatophenylpropane (BCE, purity > 99.5%) was purchased from Yangzhou Technical Material Co., Ltd. Bisphenol A epoxy resin (E51, epoxy value of 0.51) was an industrial product and provided by Nantong Xingchen Synthetic

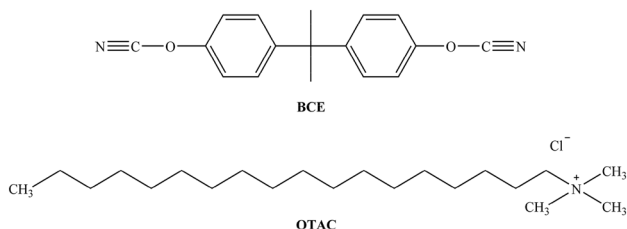


Fig. 1 Chemical structures of BCE and OTAC

Material Co., Ltd. Aluminum isopropoxide was from Tianjin Fuchen Chemical reagent factory, chemically pure. Isopropanol was from Dongguan Spartan Reagent Co., Ltd, analytical pure. Na-montmorillonite (MMT) was obtained from Henan Yongshun Purification Materials Co., Ltd. Octadecyl trimethyl ammonium chloride (OTAC) was purchased from Shanghai Shengxuan Biology Chemical Co., Ltd, analytical reagent. The chemical structures of BCE and OTAC are shown in Fig. 1.

2.2 Preparation of Al_2O_3 with sol-gel method

Aluminum isopropoxide (20 g), isopropanol (100 mL) and deionized water (40 mL) were mixed and stirred in a water bath at 80 °C for 2 h to sufficiently hydrolyze aluminum isopropoxide. The isopropanol and deionized water were removed by reduced pressure distillation, and the solid was dried at 120 °C and calcined at 700 °C for 3 h to obtain Al_2O_3 . The preparation process is shown in Fig. 2.

2.3 Modification of MMT

5 g MMT was added into a three-necked flask containing distilled water and heated and stirred at 80 °C for 2 h. In the meantime, weigh some OTAC and dissolve it with 30 mL ethanol, and then drip the solution into the above three-necked bottle and continue stirring for 5 h. After cooling the blend to room temperature, suction filtration was repeated using distilled water, and Cl^- in the filtrate was detected with $0.1 \text{ mol L}^{-1} \text{ AgNO}_3$ solution to ensure that the wet solid did not contain NaCl. The obtained wet solid was dried at 80 °C for 24 h and passed through a 200-mesh sieve to obtain OMMT. The preparation process is shown in Fig. 3.

2.4 Synthesis of E51-BCE

The mass ratio of E51 to BCE was set to 2:8. E51 was preheated to 80 °C and BCE was added into E51. Then

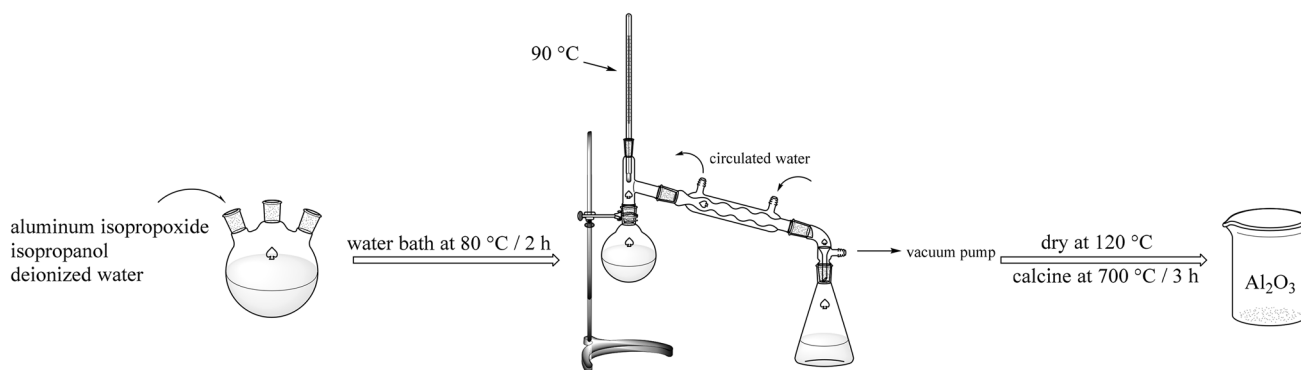


Fig. 2 The preparation process of Al_2O_3 with sol-gel method

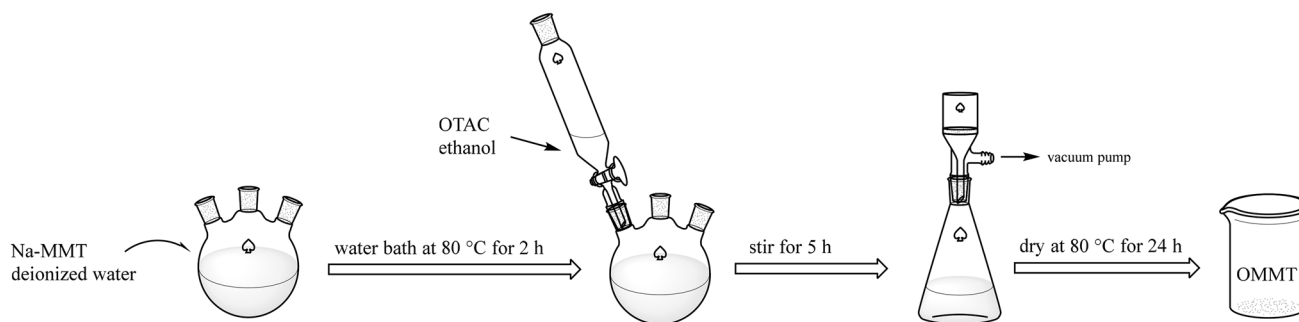


Fig. 3 The preparation process of OMMT

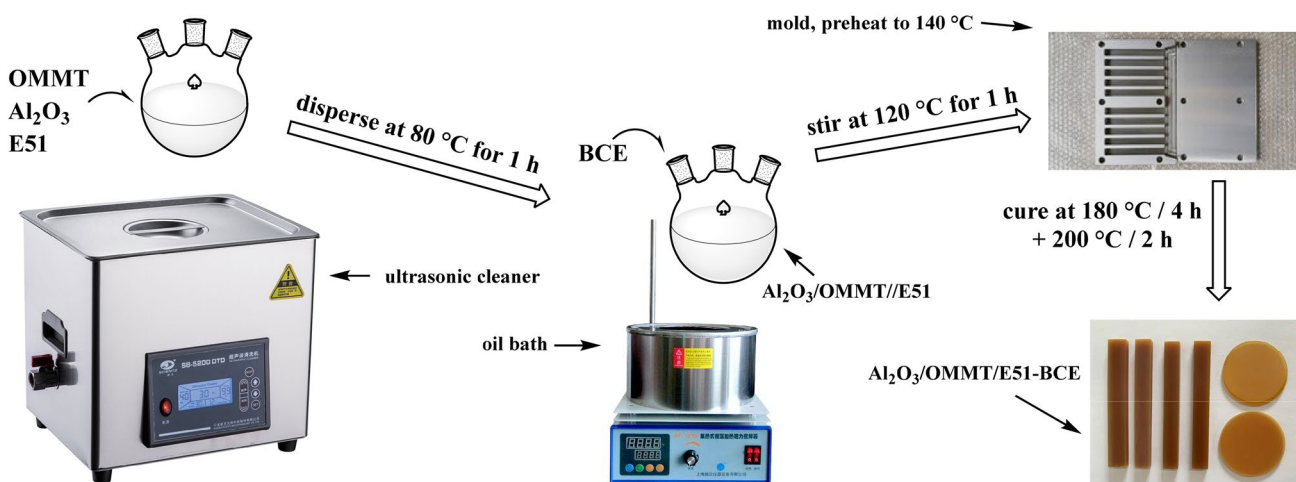


Fig. 4 The preparation process of the $\text{Al}_2\text{O}_3/\text{OMMT}/\text{E51}$ -BCE composite materials

the mixed system was heated to 120 °C and kept for 1 h. After that, the mixed system was poured into a mold which had been preheated to 140 °C and cured at 180 °C/4 h + 200 °C/2 h to obtain the modified cyanate material (E51-BCE).

2.5 Preparation of $\text{Al}_2\text{O}_3/\text{OMMT}/\text{E51}$ -BCE composite materials

Al_2O_3 and OMMT were added into E51 and ultrasonically dispersed for 1 h at 80 °C, and BCE was added into the above system to prepare $\text{Al}_2\text{O}_3/\text{OMMT}/\text{E51}$ -BCE composites, according to 180 °C/4 h + 200 °C/2 h procedure. The preparation process is presented in Fig. 4, and the samples are numbered as shown in Table 1.

2.6 Measurements

The Fourier-transform infrared spectrometer (FT-IR, EQUINOX-55, Bruker, Germany) is used to track the chemical reactions in the process of curing and study the chemical

Table 1 The component and number of samples

No	Component	Component mass ratio/ wt%	
		OMMT	Al_2O_3
A	E51-BCE	0	0
B	$\text{Al}_2\text{O}_3/\text{E51}$ -BCE	0	3
C	OMMT/E51-BCE	2	0
D1	$\text{Al}_2\text{O}_3/\text{OMMT}/\text{E51}$ -BCE	2	1
D2	$\text{Al}_2\text{O}_3/\text{OMMT}/\text{E51}$ -BCE	2	2
D3	$\text{Al}_2\text{O}_3/\text{OMMT}/\text{E51}$ -BCE	2	3
D4	$\text{Al}_2\text{O}_3/\text{OMMT}/\text{E51}$ -BCE	2	4
D5	$\text{Al}_2\text{O}_3/\text{OMMT}/\text{E51}$ -BCE	2	5

structure of the materials, and the range of spectrometer is 400–4000 cm^{-1} .

The X-ray diffraction (XRD, X'Pert Pro, Panalytical, Netherlands) is used to detect the crystal structure of Al_2O_3 , OMMT and the composites. The X-ray source is the Cu target with a generator voltage of 40 kV and a tube current of 40 mA. The wavelength of the X-ray is 0.15406 nm. Before the test,

the mixture of Al_2O_3 and OMMT is ultrasonically dispersed in ethanol for 1 h, and sieved with a 200-mesh sieve after being dried.

Thermogravimetric analysis (TGA), which not only can investigate the state of a material and the process of decomposition but also can provide useful information about the thermal stability of material, is recorded on a Pekin-Elmer 6 series thermal analysis system (USA), and samples are heated from 200 to 900 °C at the heating rate of 20 °C min^{-1} in a nitrogen atmosphere and the weight of sample was about 10–15 mg.

Micromorphology of Al_2O_3 and OMMT was characterized by transmission electron microscope (TEM, JEM-2100, JEOL, Japan). The mixture of Al_2O_3 and OMMT is ultrasonically dispersed in ethanol for 1 h before being tested.

The fracture micromorphology of the composites is observed using a scanning electron microscope (SEM, ZEISS, Germany) to clarify the dispersion of Al_2O_3 and OMMT in the matrix resin. The composites are deposited on a sample holder with adhesive carbon foil and sputtered with gold before being examined.

The dielectric constant (ϵ) and dielectric loss ($\tan\delta$) of the composite materials are measured with a broad band dielectric spectroscopy (Novocontrol Alpha-a, Germany) in the frequency range of 100 Hz–00 kHz at room temperature according to GB/T 1409-2006.

The volume resistivity of the composites is tested with a ZC-36 high resistance meter (Shanghai Precision Instruments Co., Ltd) at room temperature.

The breakdown strength of the composites is measured with a CS2674C dielectric strength tester (Nanjing) in silicone oil at room temperature, according to GB/T 1408-89. The rate of voltage is 1 kV s^{-1} .

The impact strength of the composite materials is measured by Charpy Impact Tester (TCJ-4, Jinan Huaxing Laboratory Equipment, China) according to the native standard of GB/T 2567-2008. The length, width and thickness of the sample are (80 ± 0.5) mm, (10 ± 0.1) mm and (4 ± 0.1) mm, respectively. For each sample, five measurements are made at least, and the average value is taken.

The bending strength and bending modulus of the samples are determined by electronic testing machine (CSS-4430, Shanghai Technical Instrument, China) according to the native standard of GB/T 2918–1998. The length, width and thickness of the sample are (80 ± 0.5) mm, (10 ± 0.1) mm and (4 ± 0.1) mm, respectively, and the span is 60 mm at a speed of 2 mm/min.

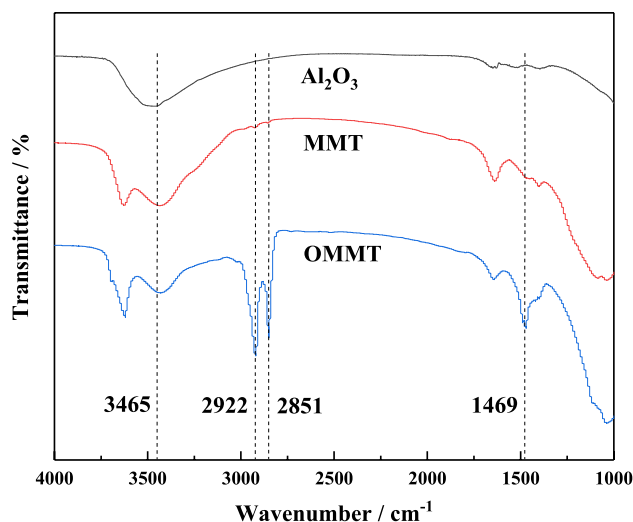


Fig. 5 FT-IR spectra of Al_2O_3 , MMT and OMMT

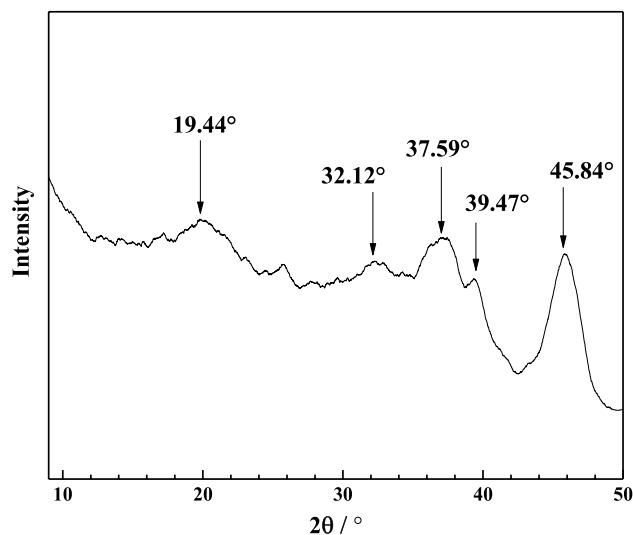


Fig. 6 XRD spectrum of Al_2O_3

3 Results and discussions

3.1 Micro-structures of Al_2O_3 and OMMT

FT-IR, XRD, TGA and TEM are usually used to analyze the micro-structures and morphology of the material. In Fig. 5, the FT-IR spectrum of Al_2O_3 shows characteristic peak of hydroxyl group at 3465 cm^{-1} [18], and the 2θ angle of $\gamma\text{-Al}_2\text{O}_3$ appears at 19.44° , 32.12° , 37.59° , 39.47° and 45.84° in the XRD spectrum of Al_2O_3 (Fig. 6, in which the curves have been smoothed to make the diffraction peaks clearer) [19, 20]. Furthermore, the shape of Al_2O_3 is confirmed to be a short fibrous crystal with

nanoscale size via its TEM image (Fig. 9a). The hydroxyl groups on the surface of γ - Al_2O_3 help to improve its compatibility with the matrix resin [21–23], which contributes to form strong two-phase interfacial and is beneficial to material properties.

FT-IR spectra of MMT and OMMT in Fig. 5 indicate the difference between MMT and OMMT; OMMT appears as new peaks at 2922 cm^{-1} , 2851 cm^{-1} and 1469 cm^{-1} , and they belong to the stretching vibration of N–H, the symmetric stretching vibration and the bending vibration of C–H in $-\text{CH}_3$ [24, 25], respectively, which indicates that the OTAC molecule interacts with MMT and is inserted into the interlayer of MMT molecular. Additionally, Fig. 7 shows XRD spectra of MMT and OMMT. It can be seen from the figure that the 001 crystal faces of MMT and OMMT appear as diffraction peaks at 6.09° and 4.12° , respectively. The distance of crystal face can be calculated using the following Braggs law:

$$2d \sin \theta = n\lambda, \quad (1)$$

where $n = 1$, $\lambda = 0.15406\text{ nm}$, d (nm) is the distance of crystal face, and θ ($^\circ$) is the angle of deviation. MMT and OMMT are the layered structures (Fig. 9b) and the crystal face distance is calculated to be 1.44 nm and 2.14 nm, respectively, indicating that the intercalator OTAC has been inserted into the interlayer of MMT and increases the crystal face distance of MMT by 48.61%. Furthermore, the content of OTAC in OMMT can be determined by TGA, and the results are presented in Fig. 8. The MMT has a residual weight of 94.33 wt% at $900\text{ }^\circ\text{C}$, and the mass loss includes the interlayer-bound water and low heat resistance structures. The mass loss of OMMT mainly occurs in the

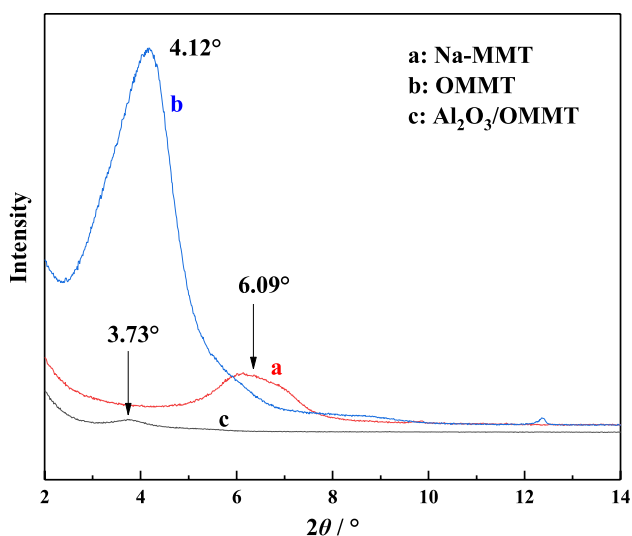


Fig. 7 XRD spectra of MMT, OMMT and $\text{Al}_2\text{O}_3/\text{OMMT}$

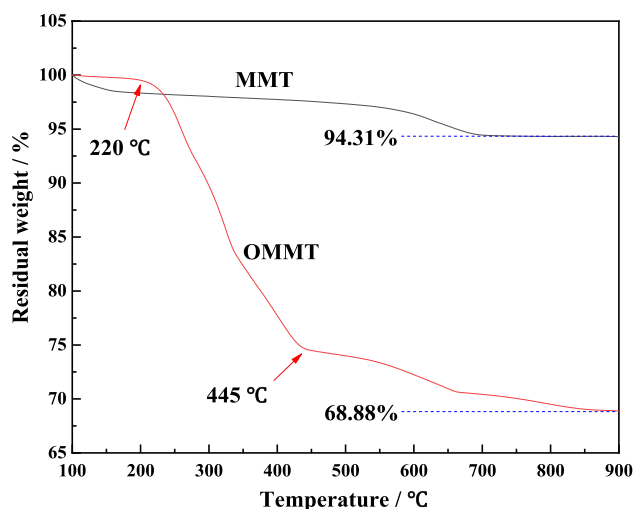


Fig. 8 TGA spectra of MMT and OMMT

range of $220\text{--}445\text{ }^\circ\text{C}$, which is mainly caused by the thermal decomposition of OTAC molecules between OMMT layers. In areas where the temperature is below $220\text{ }^\circ\text{C}$, the mass loss of OMMT, which corresponds to the loss of bound water between layers, is extremely small, which indicates that OMMT has weak hydrophilicity. When the temperature is higher than $445\text{ }^\circ\text{C}$, the mass loss of OMMT is no longer obvious. This is because the decomposition of OTAC causes the OMMT sheet to collapse, and the thermal vibration of the OTAC molecules is restricted, so the rate of thermal decomposition decreases [26]. The residual weight of OMMT is 68.88 wt% at $900\text{ }^\circ\text{C}$. The mass loss of OMMT includes the intercalator OTAC, the interlayer-bound water and the low heat resistance structure of MMT itself. The mass loss of OMMT at $900\text{ }^\circ\text{C}$ is corrected by using MMT as the control group, and the content of OTAC in OMMT is calculated to be about 25.45 wt%.

It can also be seen from XRD spectrum of $\text{Al}_2\text{O}_3/\text{OMMT}$ mixture in Fig. 7c that the diffraction peak of OMMT shifted to 3.73° , and the crystal face distance of OMMT is 2.37 nm, which means the crystal face distance of OMMT is further increased by 10.75% compared with pure OMMT. However, according to the TEM images of Al_2O_3 , OMMT and their blend, as shown in Fig. 9, it is theoretically impossible for Al_2O_3 to be inserted into OMMT layers for the diameter of Al_2O_3 (about 5 nm) is larger than the crystal face distance of OMMT (2.14 nm). The reason could be that the absorption of Al_2O_3 changes the charge distribution of OMMT layers, which weakens the electrostatic absorption between the layers.

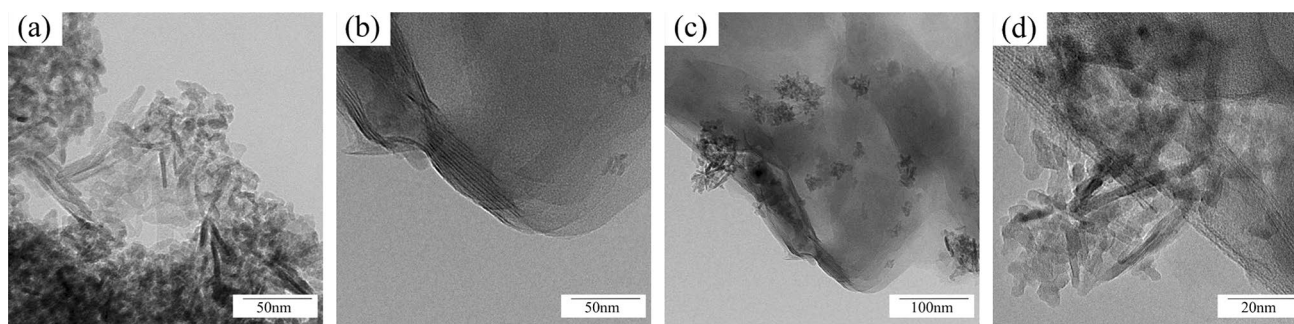


Fig. 9 TEM images of Al₂O₃, OMMT and Al₂O₃/OMMT. a Al₂O₃, b OMMT, c, d Al₂O₃/OMMT

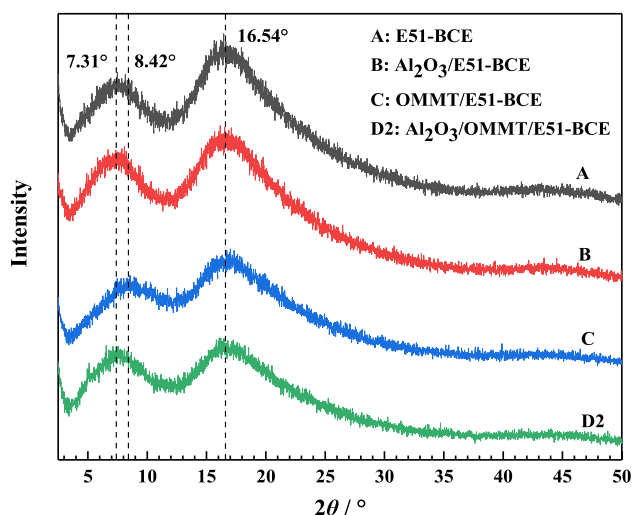


Fig. 10 XRD spectra of the E51-BCE and its related composites

Table 2 The crystallization parameters of sample (calculated by MDI Jade.)

No	Crystallinity/%	Crystallite size/nm
A	5.69	10.3
B	4.19	6.7
C	3.36	1.2
D2	4.13	3.5

3.2 Micro-structures of Al₂O₃/OMMT/E51-BCE composites

3.2.1 Crystallization characteristic of Al₂O₃/OMMT/E51-BCE composites

Figure 10 shows the XRD spectra of four kinds of composites, and the crystallization parameters are exhibited in Table 2. In Fig. 10, the XRD diffraction peaks of the reinforcement disappeared. Because OMMT is peeled into a single-layer structure in E51-BCE matrix and no longer generated the diffraction effect, at the same time, the original

crystal structure of Al₂O₃ is destroyed due to the chemical bond or electrostatic absorption with the E51-BCE matrix resin. Also, comparing the XRD spectra of the sample B, C and D2 with the sample A, it is indicated that Al₂O₃ or the mixture of Al₂O₃ and OMMT has not changed the basic crystal structure of E51-BCE, while OMMT makes the diffraction peak of sample A at 7.31° shift to the right about 1.11°, which means the crystal face distance of the matrix resin becomes smaller. The crystallization parameters of E51-BCE and its composites have exhibited that Al₂O₃, OMMT and their mixture all make the crystallinity and the crystallite size of E51-BCE decrease, and OMMT has the greatest impact. The decrease in crystallinity of the composites can contribute to improve the mechanical properties and dielectric properties of the composite materials [27].

3.2.2 Micromorphology of Al₂O₃/OMMT/E51-BCE composites

The fracture surface (SEM) images are exhibited in Fig. 11, including E51-BCE, Al₂O₃/E51-BCE, OMMT/E51-BCE and Al₂O₃/OMMT/E51-BCE composite. From Fig. 11a1, a2, the fracture surface of E51-BCE is basically typical brittle fracture, which are smooth and consistent fracture lines, indicating that energy is not obstructed during the transfer process [28], and the smooth “coastline” structure absorbed a part of fracture energy applied to the composite. In Fig. 11b1, b2, the fracture surface of Al₂O₃/E51-BCE composites is covered with squamous cracks due to the introduction of Al₂O₃; for the front of the cracks cannot break through the two-phase interaction between Al₂O₃ and E51-BCE matrix resin, the cracks are forced to separate and change the developing direction. So, the toughness of the composite materials enhances. As for the OMMT/E51-BCE and the Al₂O₃/OMMT/E51-BCE, shown in Fig. 11c1–d2, the fracture surface morphology of these two systems is much different from that of the Al₂O₃/E51-BCE. This is because the OMMT is in the disorderly dispersed status and will be pulled out from the E51-BCE matrix resin to generate deep dimples in the fracture surface, in the process of fracture.

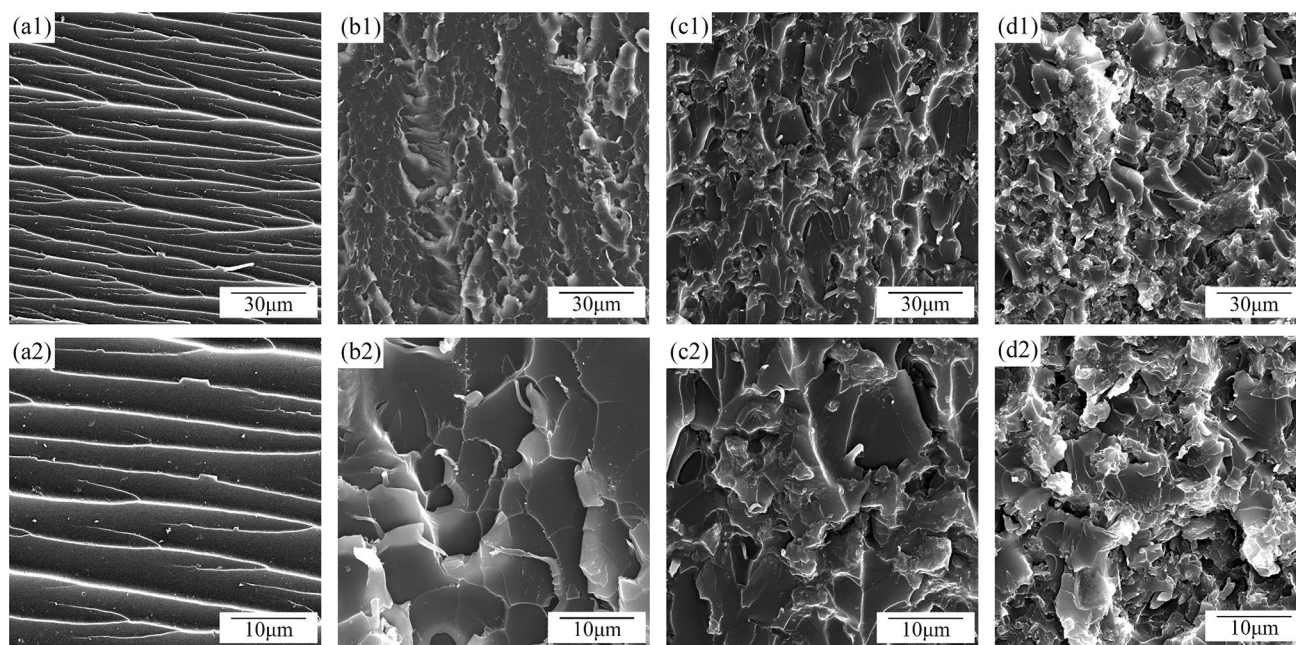


Fig. 11 SEM images of the sample. **a1, a2** Sample A (E51-BCE matrix resin), **b1, b2** Sample B ($\text{Al}_2\text{O}_3/\text{E51-BCE}$), **c1, c2** Sample C (OMMT/E51-BCE), **d1, d2** Sample D2 ($\text{Al}_2\text{O}_3/\text{OMMT}/\text{E51-BCE}$)

In the meantime, comparing OMMT/E51-BCE with $\text{Al}_2\text{O}_3/\text{OMMT}/\text{E51-BE}$, the introduction of Al_2O_3 further refines the cracks and deepens the dimples, and the development direction of cracks cannot be seen any more. The smaller cracks and deeper dimples mean that more energy has been absorbed in the break process of the composite materials, so the OMMT/ $\text{Al}_2\text{O}_3/\text{E51-BCE}$ presents the best toughness.

3.3 Mechanical properties of $\text{Al}_2\text{O}_3/\text{OMMT}/\text{E51-BCE}$

The bending strength and bending modulus of $\text{Al}_2\text{O}_3/\text{OMMT}/\text{E51-BCE}$ composites are presented in Fig. 12, and the impact strength is exhibited in Fig. 13. From two figures, both Al_2O_3 and OMMT contribute significantly to improve the mechanical properties of the E51-BCE matrix resin, and the impact of OMMT (Sample C) is greater than Al_2O_3 (Sample B), which is consistent with the characteristic in the fracture morphology of the composite materials. The bending strength, bending modulus and impact strength of Sample B are improved by 24.4%, 22.1% and 55.1% compared with the sample A, and those properties of sample C are improved by 31.1%, 50% and 108.6%, respectively. The main reasons maybe that, on the one hand, the OMMT layers form much more stronger two-phase interfacial interaction with the E51-BCE matrix resin than the Al_2O_3 particles could do [29, 30]; those interfaces absorb lots of mechanical energy when the composite materials are subjected to external forces, which improve the strength and toughness of the composites; on the other hand, due to the lower crystallinity

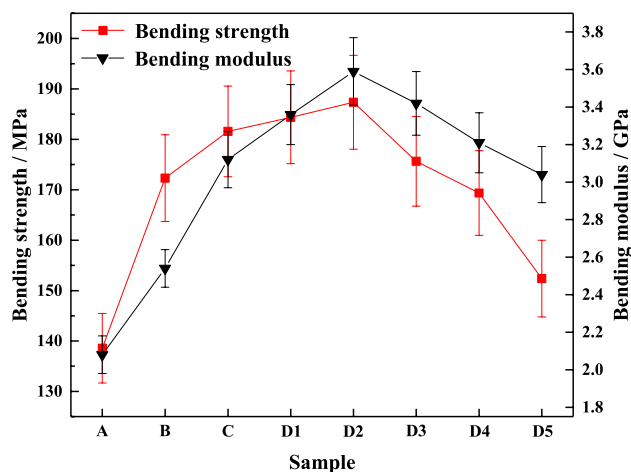


Fig. 12 Bending strength and bending modulus of $\text{Al}_2\text{O}_3/\text{OMMT}/\text{E51-BCE}$ composites

and smaller crystallite size (Table 2), the molecular structure of OMMT/E51-BCE is in a more disordered state, and the disorder of molecular structure can help to improve the toughness of the composites [31]. Additionally, sample D2 (2 wt% Al_2O_3 , 2% OMMT) shows excellent mechanical properties; the bending strength, bending modulus and impact strength are 187.34 MPa, 3.59 GPa and 35.12 kJ m^{-2} , which are 35.2%, 72.6% and 124.6% higher than those of sample A, respectively, and also obviously higher than those of sample B and sample C too. It is supposed that the

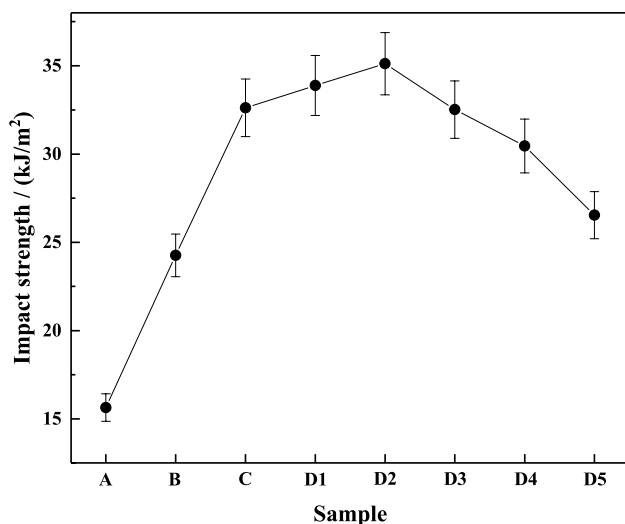


Fig. 13 Impact strength of Al₂O₃/OMMT/E51-BCE composites

introduction of Al₂O₃ increases the number of phase interfaces when the Al₂O₃ content is appropriate [32]; the effect of those phase interfaces are enough to increase the mechanical properties of the composite, although the crystallinity of Al₂O₃/OMMT/E51-BCE is higher than that of OMMT/E51-BCE. However, when the Al₂O₃ content is over 2wt%, the total content of inorganic nanoparticles in the composite material will be too high, and agglomeration phenomenon happens between the inorganic nanoparticles, which is not beneficial to improve the mechanical properties of the composites.

3.4 Dielectric properties Al₂O₃/OMMT/E51-BCE composites

3.4.1 Dielectric constant and dielectric loss

Figures 14 and 15 present the dielectric constant and dielectric loss of Al₂O₃/OMMT/E51-BCE composites. The dielectric constant and dielectric loss of sample D2 are 3.4 and 0.005 at 100 Hz, respectively. The results indicate that both dielectric constant and dielectric loss of Al₂O₃/E51-BCE composite are lower than those of the OMMT/E51-BCE material. The reason is that the interfacial polarization inside the OMMT/E51-BCE is stronger, due to the formation of more interfaces between the OMMT and the matrix resin, which causes the dielectric constant and the dielectric loss of the OMMT/E51-BCE to increase [33]. And, the dielectric constant of the composite materials gradually decreases with the increase of frequency, and the frequency dependence of dielectric constant conforms to the general characteristics of resin materials. Also, the dielectric constant of Al₂O₃/OMMT/E51-BCE composites exhibits dependence on the Al₂O₃ content, and sample D2 shows the minimum. When

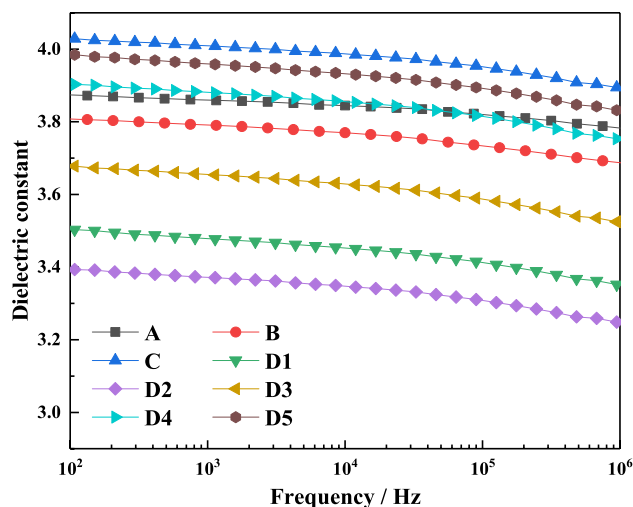


Fig. 14 Dielectric constant of the Al₂O₃/OMMT/E51-BCE composites

the Al₂O₃ content exceeds 2 wt%, the dielectric constant of the Al₂O₃/OMMT/E51-BCE composites is higher than that of the matrix resin, because the excessive Al₂O₃ creates interfacial polarization with both the E51-BCE matrix resin and the OMMT component. This indicates that the appropriateness of the inorganic component content is important to the properties of the composite materials.

Figure 15 indicates that the dielectric loss has significant dependence on the frequency and inorganic fillers. The dielectric loss is relatively stable, when the frequency is lower than 10⁴ Hz, but the dielectric loss increases obviously as the frequency is higher than 10⁴ Hz. Additionally, the dielectric loss of Al₂O₃/OMMT/E51-BCE does not increase monotonically with the increase of Al₂O₃ content, and the D2 shows

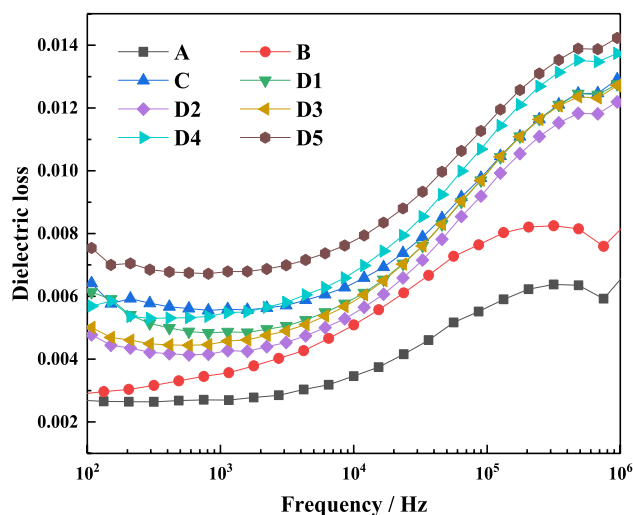


Fig. 15 Dielectric loss of the Al₂O₃/OMMT/E51-BCE composites

Table 3 The breakdown strength and volume resistivity of sample

No	Breakdown strength		Volume resistivity	
	Value/kV mm ⁻¹	Increase ratio/%	Value/ $\times 10^{13}$ Ω m	Increase magnification
A	13.33	–	1.75	–
B	14.67	10.05	112	63
C	15.06	12.98	0.55	– 0.68
D1	17.23	29.26	53	29.29
D2	19.53	46.51	89	49.86
D3	16.24	21.83	70	39
D4	15.05	12.91	61	33.86
D5	13.87	4.05	36	19.57

lower dielectric loss than that of the Sample D1, D3, D4 and D5. This is because that the dielectric loss of Al₂O₃/OMMT/E51-BCE composite materials is mainly influenced by the steering polarization of the matrix resin, thermionic polarization inside the OMMT layer and interfacial polarization between two phases, and the appropriate content of Al₂O₃ may restrict the thermionic polarization and the interfacial polarization, due to the electrostatic adsorption characteristics of Al₂O₃. So, the dielectric loss of the composites decreases.

3.4.2 Breakdown strength and volume resistivity

The breakdown strength and volume resistivity of the Al₂O₃/OMMT/E51-BCE composites are exhibited in Table 3, and sample D2 is 19.53 kV mm⁻¹ and 8.9×10^{14} Ω m, increasing by 46.51% and 50 times, respectively, compared with sample A. In the meantime, OMMT component gives the composite materials (sample C) better breakdown strength, while Al₂O₃ contributes more to improve the volume resistivity of the composite materials (sample B). The reasons are mainly that the layered structure of OMMT helps to increase the scattering of accelerated electrons inside the composite in the high voltage electric field to improve the breakdown strength of the composite materials [34]. However, ionic bonds inside OMMT lead to the increase of the ionic conductance of the composite materials, so the volume resistivity decreases [35]; the effect is opposite to that of Al₂O₃ with stable covalent bond structure. As for the sample D2, moderate amount of Al₂O₃ further enhances the electron scattering inside the composites to improve the breakdown strength of the Al₂O₃/OMMT/E51-BCE [36, 37] and counteract the negative effect of OMMT on volume resistivity, and also Al₂O₃ itself has stable covalent bond and is hard to generate free electrons in the electric field; this helps to reduce the electronic conductance inside the composite materials. However, excessive Al₂O₃ may cause the inorganic nanoparticles inside

the composites to contact each other and form conducting bridges [38], so that the volume resistivity of the composite greatly decreases. In general, both OMMT and Al₂O₃ can significantly improve insulating properties of the composite materials.

4 Conclusions

In this paper, Al₂O₃ (sol–gel method) and the OMMT (modified by OTAC) were used as reinforcements, and E51-BCE as matrix resin to prepare Al₂O₃/OMMT/E51-BCE composite. The analyzing results of microstructure exhibited that the intercalation agent OTAC can effectively increase the crystal face distance of the MMT, and Al₂O₃ is a short fibrous crystal and its presence can further increase the crystal face distance of the OMMT, which made it easier for the matrix resin to enter the Al₂O₃/OMMT layer. The good compatibility of Al₂O₃/OMMT with E51-BCE matrix resin made small cracks and deep dimples on the fracture surface of the Al₂O₃/OMMT/E51-BCE composites when the composites were subjected to external forces, and contributed to improve both mechanical and dielectric properties of the composites. When both Al₂O₃ and OMMT contents were 2wt%, the Al₂O₃/OMMT/E51-BCE composites show the highest values of 187.34 MPa in bending strength, 3.59 GPa in bending modulus, 35.12 kJ m⁻² in impact strength, 19.53 kV mm⁻¹ in breakdown strength and 8.9×10^{14} Ω m in volume resistivity; the dielectric constant and dielectric loss tangent of the composite are 3.4 and 0.005, respectively, at the electric field frequency of 100 Hz. The Al₂O₃/OMMT/E51-BCE composites had both excellent mechanical and dielectric properties, which could meet the requirements in the insulating materials field.

Acknowledgements The authors would like to express their appreciation to the project support by the National Natural Science Foundation of China (Grant No. 51603057) and the Harbin technology bureau subject leader (Grant No. 2015RAXXJ029).

Data availability All data included in this study are available from the corresponding author upon reasonable request.

Compliance with ethical standards

Conflict of interest The authors declare that there are no conflicts of interest regarding the publication of this paper.

References

1. J.F. Zhou, J.J. Wang, J.Q. Zhao, K.K. Jin, J. Sun, X.J. Guo, Q. Fang, Polym. Chem. **8**, 6173 (2017)
2. L.H. Zheng, L. Yuan, Q.B. Guan, A.J. Gu, G.Z. Liang, High Volt. **2**, 32 (2017)

3. A. Bauer, M. Thunga, K. Obusek, M. Akinc, M.R. Kessler, *Polymer* **54**, 3994 (2013)
4. X. Sheng, M. Akinc, M.R. Kessler, *Mater. Sci. Eng. A* **527**, 5892 (2010)
5. Y. Zhang, L. Yuan, F. Chen, A.J. Gu, G.Z. Liang, *Polym. Bull.* **74**, 1011 (2016)
6. S.Y. Chen, Y.H. Cheng, Q. Xie, B. Xiao, Z.D. Wang, J.Y. Liu, G.L. Wu, *Compos. A* **120**, 84 (2019)
7. N.P. Maity, R.R. Thakur, R. Maity, R.K. Thapa, S. Baishya, *Appl. Mech. Mater.* **860**, 25 (2016)
8. J.L. Li, J.H. Yin, C. Yang, N. Li, Y. Feng, Y.Y. Liu, H. Zhao, Y.P. Li, C.C. Zhu, D. Yue, B. Su, X.X. Liu, *J. Polym. Sci. B* **57**, 574 (2019)
9. J.H. Park, E. Hong, S.H. An, D.H. Lim, C.H. Shin, *Korean J. Chem. Eng.* **34**, 2610 (2017)
10. C.H. Lin, B.W. Wang, H.T. Guo, L.G. Chen, X.L. Yan, *Bull. Korean Chem. Soc.* **39**, 391 (2018)
11. W.G. Fu, X. Zhang, Y.Y. Mao, T.F. Pei, B.S. Sun, S.Z. Mei, L. Chen, *Ceram. Int.* **44**, 15824 (2018)
12. Z.R. Jia, Z.G. Gao, D. Lan, Y.H. Cheng, G.L. Wu, H.J. Wu, *Chin. Phys. B* **27**, 117806 (2018)
13. D.A. Kissounko, J.M. Deitzel, S.P. Doherty, A. Shah, J.W. Gillespie, *Eur. Polym. J.* **44**, 2807 (2008)
14. Y. Lin, M. Song, C.A. Stone, S.J. Shaw, *Thermochim. Acta* **552**, 77 (2013)
15. X. Jian, W. Xuebing, D. Bingyao, L. Qingsheng, *High Perform. Polym.* **28**, 618 (2016)
16. C.C. Chou, Y.C. Chang, M.L. Chiang, J.J. Lin, *Macromolecules* **37**, 473 (2004)
17. H.P. He, R.L. Frost, T. Bostrom, P. Yuan, L. Duong, D. Yang, X.F. Yunfel, J.T. Klopogge, *Appl. Clay Sci.* **31**, 262 (2006)
18. A.L. Feng, G.L. Wu, Y.Q. Wang, C. Pan, *J. Nanosci. Nanotechnol.* **17**, 3859 (2017)
19. Z.M. Liu, J.W. Wang, M.Q. Kang, N. Yin, X.K. Wang, Y.S. Tan, Y.L. Zhu, *J. Braz. Chem. Soc.* **25**, 152 (2013)
20. F.M. Segal, M.F. Correa, R. Bacani, B. Castanheira, M.J. Politi, S. Brochsztain, E.R. Triboni, *Mater. Res.* **21**, 36–38 (2018)
21. X. Sheng, M. Akinc, M.R. Kessler, *Polym. Eng. Sci.* **50**, 302 (2010)
22. I. Czekaj, J. Wambach, O. Krocher, *Int. J. Mol. Sci.* **10**, 4310 (2009)
23. J.E. Park, B.B. Kim, E.D. Park, *Korean J. Chem. Eng.* **32**, 2212 (2015)
24. S. Nagendiran, C. Chinnakkannu Karikal, M. Alagar, I. Hamerton, *High Perform. Polym.* **20**, 323 (2007)
25. V. Bershtein, A. Fainleib, L. Egorova, K. Gusakova, O. Grigoryeva, D. Kirilenko, S. Konnikov, V. Ryzhov, P. Yakushev, N. Lavrenyuk, *Nanoscale Res. Lett.* **10**, 165 (2015)
26. Y.F. Xi, Z. Ding, H.P. He, R.L. Frost, *J. Colloid Interface Sci.* **277**, 116 (2004)
27. Z. Liu, L. Yuan, G.Z. Liang, A.J. Gu, *Polym. Adv. Technol.* **26**, 1608 (2015)
28. A.L. Feng, G.L. Wu, C. Pan, Y.Q. Wang, *J. Nanosci. Nanotechnol.* **17**, 3786 (2017)
29. S. Nagendiran, S. Premkumar, M. Alagar, *J. Appl. Polym. Sci.* **106**, 1263 (2007)
30. A. Akelah, A. Rehab, E.R. Kenawy, M.S. Abou Zeid, *J. Appl. Polym. Sci.* **101**, 1121 (2006)
31. I. Mondragón, L. Solar, A. Nohales, C.I. Vallo, C.M. Gómez, *Polymer* **47**, 3401 (2006)
32. G.L. Wu, Y.H. Cheng, K.K. Wang, Y.Q. Wang, A.L. Feng, *J. Mater. Sci.-Mater. Electron.* **27**, 5592 (2016)
33. F.C. Lü, H.O. Ruan, J.X. Song, K. Yin, Z.Y. Zhan, Y.F. Jiao, Q. Xie, *J. Phys. D* **52**, 155201 (2019)
34. X.H. Zhang, Z.X. Shi, L.S. Ma, J.G. Gao, N. Guo, *J. Appl. Polym. Sci.* **136**, 47364 (2019)
35. A.L. Feng, T.Q. Hou, Z.R. Jia, Y. Zhang, F. Zhang, G.L. Wu, *Nanomaterials* **10**, 162 (2020)
36. X.Y. Huang, F. Liu, P.K. Jiang, *IEEE Trans. Dielectr. Electr. Insul.* **17**, 1697 (2010)
37. D.L. Ma, R.W. Siegel, J.I. Hong, L.S. Schadler, E. Martensson, C. Onneby, *J. Mater. Res.* **19**, 857 (2004)
38. Y.Q. Wang, G.L. Wu, K.C. Kou, C. Pan, A.L. Feng, *J. Mater. Sci.-Mater. Electron.* **27**, 8279 (2016)

Publisher's Note Springer Nature remains neutral with regard to jurisdictional claims in published maps and institutional affiliations.